Australian Government
Department of Defence
Defence Science and
Technology Organisation

Design of Optimal Flight Controller for Generic Linearised Missile Model in Hypersonic Regime

Jijoong Kim and Farhan A. Faruqi

Weapons Systems Division
Defence Science and Technology Organisation

DSTO-TR-2423

ABSTRACT

This report presents a multivariable controller design for a generic missile travelling at hypersonic speed. The controller is based on the theory of optimal control, and the solution is provided by a feedback controller known as a Linear Quadratic Regulator (LQR) for tracking the demands (lateral acceleration and roll rate) as closely as possible while keeping the actuator efforts (for deflecting aileron, elevator and rudder) small. In the computer simulation, the missile model is subject to various hypersonic flight conditions and gain scheduling is exercised as a function of dynamic pressure. The intial study assumes perfect knowledge of all the states for the controller design. Subsequently, a state observer (kalman filter) is introduced into the design to reflect a more practical synthesis where some of the states need to be estimated.

Published by

Weapons Systems Division
DSTO Defence Science and Technology Organisation
PO Box 1500
Edinburgh South Australia 5111 Australia

Telephone: (08) 7389 5555
Fax: (08) 7389 6567

AR-017-787
July 2010

APPROVED FOR PUBLIC RELEASE

Design of Optimal Flight Controller for Generic Linearised Missile Model in Hypersonic Regime

Executive Summary

The design of a missile autopilot controller that provides a fast and stable response to guidance commands and also maintains the performance throughout the entire flight envelope, poses a challenge to the flight control engineer. This report considers the autopilot design for a generic cruciform missile utilising the generic 6DoF airframe model developed in-house [Faruqi 2007] and the linear quadratic regulator (LQR) technique.

The control designs are presented for tracking the desired lateral accelerations and roll rate, where the control inputs are aileron, elevator and rudder deflections. The optimal LQR design aims to find the feedback gain that minimises a particular cost function. In this case it is the weighted sum of energies associated with tracking error and control signal. Note that these two cost terms are conflicting (i.e., faster tracking leads to increased strain on the actuator) and the role of the control gain is simply a trade-off between the response time and control effort.

We subject the vehicle to two hypersonic flight conditions and show that a gain scheduling may be performed using the dynamic pressure as the sole scheduling input. The controller design extends to output feedback control where a state observer is included in the feedback loop.

Authors

Jijoong Kim
Weapons Systems Division

Jijoong Kim received a B.E. (Hons) in Electrical and Electronic Engineering and M.EngSc. both from the University of Adelaide in 1993 and 1995, respectively. He was a research assistant at the EE department of the University of Adelaide for six months, and then joined DSTO in November 1995. He also received PhD from the University of Wollongong 2005. Since 1995, he has been with the Guidance and Control Group. His research interests include: Missile Guidance, Optimal Control, Inertial Navigation and GPS, and Computer Vision

Farhan A. Faruqi
Weapons Systems Division

Farhan received B.Sc(Hons) in Mechanical Engineering from the University of Surrey (UK) , 1968, M.Sc in Automatic Control from the University of Manchester Institute of Science and Technology (UK), 1970 and Ph.D from the Imperial College, London University (UK), 1973. He has over 20 years experience in the Aerospace and Defence Industry in UK, Europe and the USA. Prior to joining DSTO in January 1999 he was an Associate Professor at QUT (Australia) 1993-98. His research interests include: Missile Navigation, Guidance and Control, Target Tracking and Precision Pointing Systems, Strategic Defence Systems, Signal Processing, and Optoelectronics.

Contents

1. Introduction

The design of a missile autopilot controller which provides a fast and stable response to guidance commands, and which maintains the performance throughout the entire flight envelope, poses a challenge to the flight control engineer. This report considers the autopilot design for a generic cruciform missile utilising the generic 6DoF airframe model developed in-house [Faruqi 2007] and the linear quadratic regulator (LQR) technique.

Classical control techniques usually involve loop shaping approaches - frequency domain techniques such as bode and Nyquist plots. Single-Input Single-Output (SISO) systems are the primary focus of classical controls. Multiple-Input Multiple-Output (MIMO) systems can be controlled through classical control techniques, but to do so usually requires that each input and output can be decoupled. In this case the system can be treated as a bunch of SISO systems and each controller can be designed without consideration of the others.

Controllers are filters that shape the feedback error to achieve the desired system response. The input to a controller is the error between the desired and measured system outputs. The controller's output is a filtered version of that error. Controller design is a matter of selecting poles, zeros, and gains. Poles provide integral action which is slow responding to errors but drives the step response to a zero steady-state error. Zeros are responsible for derivative action which is fast but can amplify noise and leads to a non-zero steady-state error. Gains provide instantaneous response to errors.

When applied to the flight control, the classical approach leads to a three-loop autopilot [Nesline and Nabbefeld 1984], where longitudinal, lateral and roll dynamics are considered independently as mentioned above. This approach is valid for a limited range of flight conditions. Furthermore, loop shaping can be very difficult for MIMO systems.

The state-based modern control design allows for a more convenient and compact way to model and analyse MIMO systems, where the inter-axial coupling effects are included. This approach can be applied to more extreme flight regimes, non-symmetrical airframes with non-symmetrical mass distribution, and adaptive control.

The optimal LQR design aims to minimise or maximise a particular cost function. In our case it is the minimisation of the combined energy of tracking error (response speed) and control signal. Note that these two cost terms are conflicting (i.e. decreasing one increases the other) and the role of control gain is simply the trade-off between the response time and control effort.

We initially assume that all 24 states are precisely known, and design a full state feedback controller. We then present the stability issue, steady state gain, effect of poles and zeros on step response, and gain scheduling for the two flight envelopes associated with the hypersonic air-to-ground attack scenarios. We then move on to the observed feedback control design, where only 6 inertial measurement unit (IMU) output variables are available, and a Kalman filter is used to estimate the 24 state variables from the 6 measurement variables. Replacing the true state variables with the estimates, we repeat some of the previous computer simulations and investigate the effect of the state observer on the closed loop response.

2. State Feedback Control System

In this section, we present the closed-loop optimal control of linear systems with quadratic performance index. This leads to the linear quadratic regulator (LQR) system dealing with state regulation (keeping the state around zero). If the requirement is altered to make the state follow or track a desired trajectory, then the problem becomes that of linear quadratic tracking (LQT) or alternatively the servomechanism problem.

2.1 Formulation

The linearised dynamical system is governed by the following differential equations

$$\dot{\mathbf{x}}(t) = \mathbf{F}(t)\mathbf{x}(t) + \mathbf{G}(t)\mathbf{u}(t) + \mathbf{w}(t) \tag{1}$$

and the measurement equations are given as

$$\mathbf{z}(t) = \mathbf{J}(t)\mathbf{x}(t) + \mathbf{v}(t)\,. \tag{2}$$

where

$\mathbf{x}$ is a 24×1 system state vector,
$\mathbf{u}$ is a 3×1 (servo) input vector $=[\xi,\eta,\zeta]^T$,
$\mathbf{z}$ is a 6×1 measurement (accelerations and body rates)vector $=[a_x,a_y,a_z,p,q,r]^T$,
$\mathbf{w}$ is a 24×1 process noise vector,
$\mathbf{v}$ is a 6×1 measurement noise vector,
$\mathbf{F}$ is a 24×24 system coefficient matrix,
$\mathbf{G}$ is a 24×3 control coefficient matrix,
$\mathbf{J}$ is a 6×24 measurement coefficient matrix.

The state vector $\mathbf{x}$ contains 24 states:
$(u,v,w,p,q,r,a_x,\dot{a}_x,a_y,\dot{a}_y,a_z,\dot{a}_z,p_o,\dot{p}_o,q_o,\dot{q}_o,r_o,\dot{r}_o,\xi_o,\dot{\xi}_o,\eta_o,\dot{\eta}_o,\zeta_o,\dot{\zeta}_o)$ where the first six elements are 3 velocity components and 3 angular rate components, the next 12 elements are the accelerometer and gyroscope outputs and their rates, and the remaining 6 elements are the control surface deflections and their rates). The derivation and detailed descriptions of the above state space model are given in [Faruqi 2007]. Figure 1 shows the step responses of the 24 states when $a_{y\_demand} = 1\text{ms}^{-2}$.

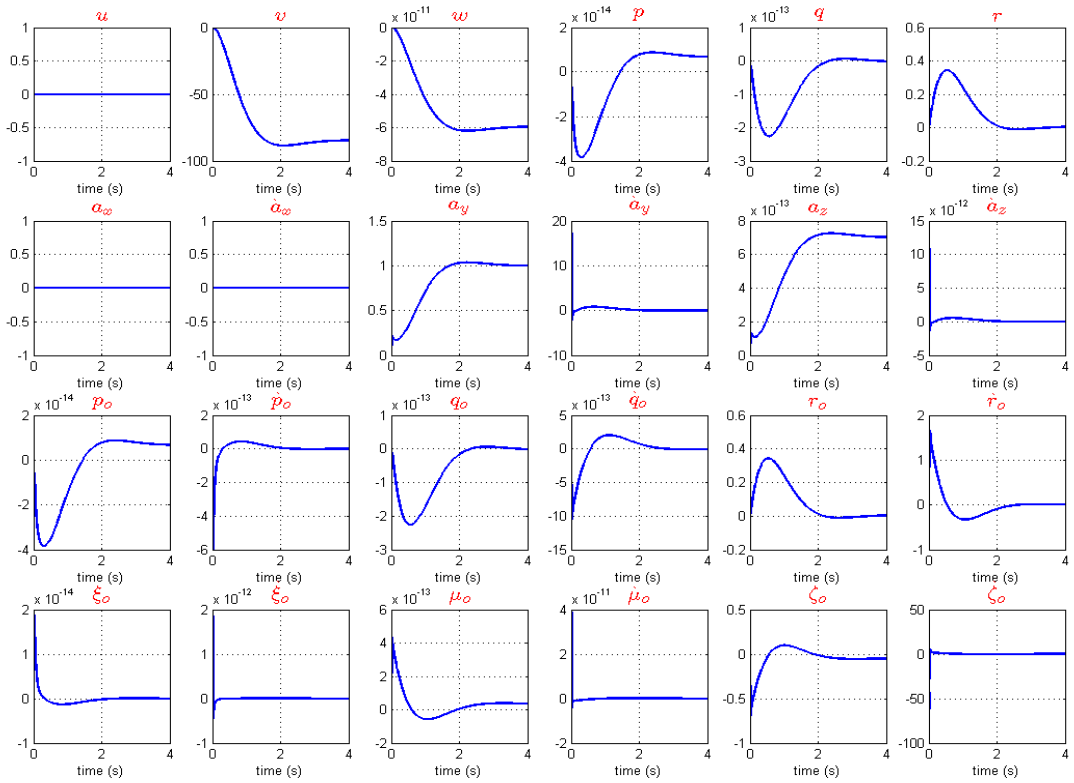

Figure 1: Step response of 24 states

Our objective is to control the system in such a way that the output $\mathbf{z}(t)$ tracks the desired output $\boldsymbol{\eta}(t)$ as closely as possible during the interval $[t_0, t_f]$ such that the cost function shown below is minimised. Let us define the error vector as $\mathbf{e}(t) = \boldsymbol{\eta}(t) - \mathbf{z}(t)$, and choose the performance index as

$$C = \frac{1}{2}\mathbf{e}^T(t_f)\mathbf{S}(t_f)\mathbf{e}(t_f) + \frac{1}{2}\int_{t_0}^{t_f}[\mathbf{e}^T(t)\mathbf{Q}(t)\mathbf{e}(t) + \mathbf{u}^T(t)\mathbf{R}(t)\mathbf{u}(t)]dt \tag{3}$$

where

$\mathbf{S}$ is a 6×6 symmetric positive semi-definite weighting matrix ,
$\mathbf{Q}$ is a 6×6 symmetric positive semi-definite weighting matrix,
$\mathbf{R}$ is a 3×3 symmetric positive definite input weighting matrix.

From now on, we omit *t* for brevity except for the initial and final time.

Taking the variational approach as in [Sage 1969; Naidu 2002], the solution to the optimal feedback control problem is given as:

$$\mathbf{u} = [-\mathbf{R}^{-1}\mathbf{G}^T\mathbf{P}]\mathbf{x} + [\mathbf{R}^{-1}\mathbf{G}^T]\boldsymbol{\xi} \tag{4}$$

where

$$\dot{\mathbf{P}} = -\mathbf{PF} - \mathbf{F}^T\mathbf{P} + \mathbf{PGR}^{-1}\mathbf{G}^T\mathbf{P} - \mathbf{J}^T\mathbf{QJ} \text{ (Differential Riccati Equation)} \quad (5)$$

$$\mathbf{P}(t_f) = \mathbf{J}^T(t_f)\mathbf{S}(t_f)\mathbf{J}(t_f) \text{ and} \quad (6)$$

$$\dot{\boldsymbol{\xi}} = -[\mathbf{F} - \mathbf{GR}^{-1}\mathbf{G}^T\mathbf{P}]^T\boldsymbol{\xi} - \mathbf{J}^T\mathbf{Q}\boldsymbol{\eta} \quad (7)$$

$$\boldsymbol{\xi}(t_f) = \mathbf{J}^T(t_f)\mathbf{S}(t_f)\boldsymbol{\eta}(t_f) \quad (8)$$

Given the final conditions (6) and (8), the differential equations (5) and (7) can be solved by integrating backwards in time (from t_f to t_0). Note that the Riccati equation (5) can also be solved analytically [Anderson and Moore 1989; Naidu 2002].

By setting $t_f = \infty$, the problem becomes the infinite time (steady-state) case, and the performance index simplifies to

$$C = \frac{1}{2}\int_{t_0}^{\infty}[\mathbf{e}^T(t)\mathbf{Q}(t)\mathbf{e}(t) + \mathbf{u}^T(t)\mathbf{R}(t)\mathbf{u}(t)]dt \quad (9)$$

The steady state $\mathbf{P}$ is obtained by solving the Continuous Algebraic Riccati Equation (CARE)

$$\mathbf{0} = -\mathbf{PF} - \mathbf{F}^T\mathbf{P} + \mathbf{PGR}^{-1}\mathbf{G}^T\mathbf{P} - \mathbf{J}^T\mathbf{QJ} \quad (10)$$

And the steady state $\boldsymbol{\xi}$ is solved by setting $\dot{\boldsymbol{\xi}} = \mathbf{0}$ and is given by

$$\boldsymbol{\xi} = -[(\mathbf{F} - \mathbf{GR}^{-1}\mathbf{G}^T\mathbf{P})^T]^{-1}\mathbf{J}^T\mathbf{Q}\boldsymbol{\eta} \quad (11)$$

We can use the analytic solution [Anderson and Moore 1989; Naidu 2002] or a matlab toolbox function "*care*" as shown below.

$$\mathbf{P} = care(\mathbf{F}, \mathbf{G}, \mathbf{J}^T\mathbf{QJ}, \mathbf{R})$$

Having found the stabilising solutions $\mathbf{P}$ and $\boldsymbol{\xi}$, the optimal feedback gain $\mathbf{K}_c$ is given as

$$\mathbf{K}_c = \mathbf{R}^{-1}\mathbf{G}^T\mathbf{P} \quad (12)$$

Adding the input gain term, the solution to the control input is written as

$$\mathbf{u} = -\mathbf{K}_c\mathbf{x} + \mathbf{K}_1\boldsymbol{\xi} \quad (13)$$

where $\mathbf{K}_1 = \mathbf{R}^{-1}\mathbf{G}^T$ (input gain matrix) (14)

We express ξ as (refer to Figure 2),

$$\xi = \mathbf{A}^{-1}\mathbf{B}\eta \tag{15}$$

where

$$\mathbf{A} = -(\mathbf{F} - \mathbf{G}\mathbf{R}^{-1}\mathbf{G}^T\mathbf{P})^T = -(\mathbf{F} - \mathbf{G}\mathbf{K}_c)^T \tag{16}$$

$$\mathbf{B} = \mathbf{J}^T\mathbf{Q} \tag{17}$$

Note that for the linear quadratic regulator (LQR) problem, the input gain term (11) is omitted and $\mathbf{J}$ term in (10) also disappears. The transient behaviour and stability of the demand tracking problem is the same as the regulator problem, therefore the stability analysis is performed in LQR context.

2.2 Stability of LQR system

Ignoring the input term, the closed loop differential equation becomes,

$$\dot{\mathbf{x}}(t) = (\mathbf{F} - \mathbf{G}\mathbf{K}_c)\mathbf{x} \tag{18}$$

In order for $\mathbf{F} - \mathbf{G}\mathbf{K}_c$ to be a stable matrix, the second method of Lyapunov [Ogata 1995] states that there must exist a positive definite matrix $\mathbf{P}$ that satisfies the following equation

$$[(\mathbf{F} - \mathbf{G}\mathbf{K}_c)^T\mathbf{P} + \mathbf{P}(\mathbf{F} - \mathbf{G}\mathbf{K}_c)] + \mathbf{X} = \mathbf{0} \tag{19}$$

where $\mathbf{X}$ is some positive definite symmetric matrix.

We know $\mathbf{Q}$ is positive semi-definite and $\mathbf{R}$ is positive definite, and they are both diagonal, hence we may say $\mathbf{Q} + \mathbf{K}_c^T\mathbf{R}\mathbf{K}_c$ is positive definite. We introduce a matrix $\mathbf{X}$ and set it as

$$\mathbf{X} = \mathbf{Q} + \mathbf{K}_c^T\mathbf{R}\mathbf{K}_c \tag{20}$$

Substituting $\mathbf{X} = \mathbf{Q} + \mathbf{K}_c^T\mathbf{R}\mathbf{K}_c$ into (19), we get

$$(\mathbf{F} - \mathbf{G}\mathbf{K}_c)^T\mathbf{P} + \mathbf{P}(\mathbf{F} - \mathbf{G}\mathbf{K}_c) + (\mathbf{Q} + \mathbf{K}_c^T\mathbf{R}\mathbf{K}_c) = \mathbf{0}. \tag{21}$$

Expanding the above equation leads to

$$\mathbf{F}^T\mathbf{P} + \mathbf{P}\mathbf{F} - \mathbf{K}_c^T\mathbf{G}^T\mathbf{P} - \mathbf{P}\mathbf{G}\mathbf{K}_c + \mathbf{Q} + \mathbf{K}_c^T\mathbf{R}\mathbf{K}_c = \mathbf{0}. \tag{22}$$

The optimal feedback gain according to the LQR design is $\mathbf{K}_c = \mathbf{R}^{-1}\mathbf{G}^T\mathbf{P}$ as in (12). Substituting $\mathbf{R}^{-1}\mathbf{G}^T\mathbf{P}$ for $\mathbf{K}_c$ in (22) leads to the following stability condition

$$\mathbf{F}^T\mathbf{P} + \mathbf{P}\mathbf{F} - \mathbf{P}\mathbf{G}\mathbf{R}^{-1}\mathbf{G}^T\mathbf{P} + \mathbf{Q} = \mathbf{0}, \tag{23}$$

This is the algebraic Riccati equation in the LQR problem that was used earlier to compute $\mathbf{P}$ which was utilised to generate $\mathbf{K}_c$ and $\mathbf{u}$. Since the necessary stability condition (i.e., the second method of Lyapunov [Ogata 1995]) leads to the Riccati equation, we may say that the proposed closed-loop system is asymptotically stable.

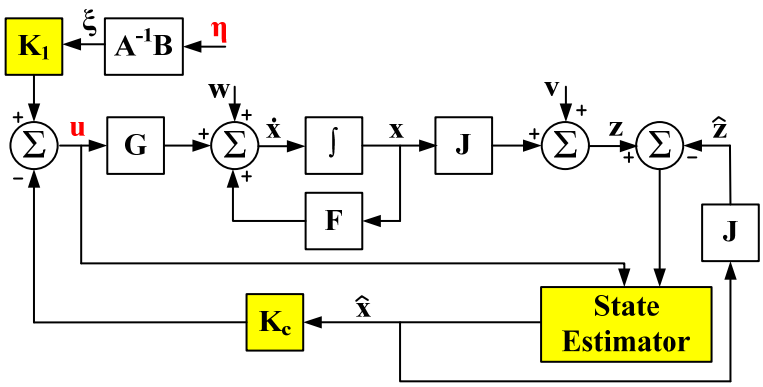

Figure 2: LQT design with Gaussian error terms and state estimator (output feedback)

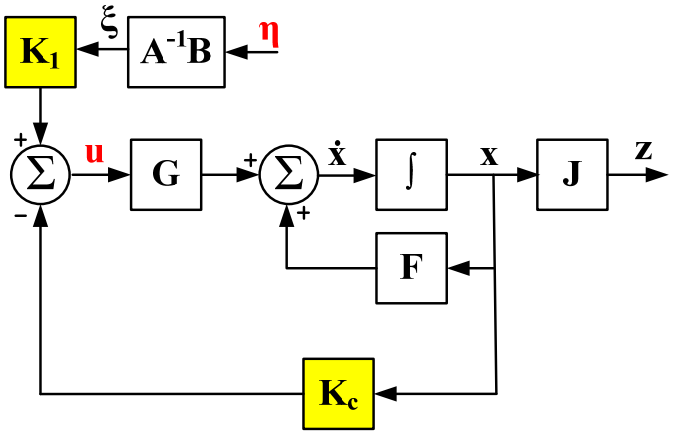

Figure 3: Error free LQT design with full state feedback

The proposed linear quadratic tracker (LQT) design with the feedback and input gains $\mathbf{K}_c$ and $\mathbf{K}_1$, and state observer is shown in Figure 2. However, the majority of the simulations in this report are based on the full-state feedback scheme as in Figure 3.

2.3 Steady State Gain

Substituting the optimal input and feedback gain terms into (1), we get the following closed-loop differential equation

$$\dot{\mathbf{x}} = [\mathbf{F} - \mathbf{G}\mathbf{K}_c]\mathbf{x} + [\mathbf{G}\mathbf{K}_1((\mathbf{G}\mathbf{K}_c - \mathbf{F})^T)^{-1}\mathbf{J}^T\mathbf{Q}]\boldsymbol{\eta}. \quad (24)$$

At steady state, $\dot{\mathbf{x}} = \mathbf{0}$, and the analytical solution for steady state $\mathbf{x}$ is given as

$$\mathbf{x} = [\mathbf{G}\mathbf{K}_c - \mathbf{F}]^{-1}\mathbf{G}\mathbf{K}_1[(\mathbf{G}\mathbf{K}_c - \mathbf{F})^T]^{-1}\mathbf{J}^T\mathbf{Q}\boldsymbol{\eta}\,. \tag{25}$$

By setting $\mathbf{R} = \mathbf{I}_{3\times 3}$, we get $\mathbf{K}_1 = \mathbf{G}^T$ (see (14)), and Equation (25) becomes

$$\mathbf{x} = [\mathbf{G}\mathbf{K}_c - \mathbf{F}]^{-1}\mathbf{G}\mathbf{G}^T[(\mathbf{G}\mathbf{K}_c - \mathbf{F})^T]^{-1}\mathbf{J}^T\mathbf{Q}\boldsymbol{\eta} \tag{26}$$

The measurement equation is

$$\begin{aligned}\mathbf{z} &= \mathbf{J}\mathbf{x}\\ &= \mathbf{J}(\mathbf{G}\mathbf{K}_c - \mathbf{F})^{-1}\mathbf{G}\mathbf{G}^T((\mathbf{G}\mathbf{K}_c - \mathbf{F})^T)^{-1}\mathbf{J}^T\mathbf{Q}\boldsymbol{\eta}\\ &= [\mathbf{J}(\mathbf{G}\mathbf{K}_c - \mathbf{F})^{-1}\mathbf{G}][\mathbf{J}(\mathbf{G}\mathbf{K}_c - \mathbf{F})^{-1}\mathbf{G}]^T\mathbf{Q}\boldsymbol{\eta}\\ &= \mathbf{T}_{ss}\boldsymbol{\eta}\end{aligned} \tag{27}$$

The steady state gain matrix $\mathbf{T}_{ss} = [\mathbf{J}(\mathbf{G}\mathbf{K}_c - \mathbf{F})^{-1}\mathbf{G}][\mathbf{J}(\mathbf{G}\mathbf{K}_c - \mathbf{F})^{-1}\mathbf{G}]^T\mathbf{Q}$ is symmetric and maps the desired output (or demand) $\boldsymbol{\eta}$ to the actual output $\mathbf{z}$ in steady state.

Typically $\mathbf{T}_{ss}$ appears as below

$$\mathbf{T}_{ss} \approx \begin{bmatrix} 0 & 0 & 0 & 0 & 0 & 0\\ 0 & 1 & 0 & 0 & 0 & 0\\ 0 & 0 & 1 & 0 & 0 & 0\\ 0 & 0 & 0 & 1 & 0 & 0\\ 0 & 0 & 0 & 0 & 0 & 0\\ 0 & 0 & 0 & 0 & 0 & 0 \end{bmatrix}.$$

The non-zero diagonal elements of $\mathbf{T}_{ss}$ represent steady state gains, a_y / a_{y_demand}, a_z / a_{z_demand} and p_o / p_{demand} in descending order. The remaining terms are either zeros or close to zero. The non-zero diagonal elements approximate to 1 only if $\mathbf{Q}$ is large. It was observed that as $\mathbf{Q}$ gets smaller, the diagonal terms get smaller as well. In order to explain this observation, we present a simple scalar differential equation.

$$\dot{x} = fx + u \tag{28}$$
$$z = x \tag{29}$$

Since $g = r = 1$, the gains become $K_c = p$ and $K_1 = 1$, then the scalar version of (25) becomes

$$\dot{x} = (f - p)x + \frac{q\eta}{p - f} \tag{30}$$

At steady state (ie., $\dot{x} = 0$),

$$x = \frac{q\eta}{(p-f)^2} \tag{31}$$

where q is a scalar weighting coefficient.

Then the measurement output becomes

$$z = x = \frac{q\eta}{(p-f)^2}. \tag{32}$$

Expanding the denominator, the gain can be shown as

$$\frac{z}{\eta} = \frac{q}{p^2 - 2pf + f^2}. \tag{33}$$

Now solving the scalar Riccati equation, $2pf - p^2 + q = 0$, we obtain the optimal q as $q = p^2 - 2pf$, therefore the above gain can be expressed as

$$\frac{z}{\eta} = \frac{q}{q + f^2}. \tag{34}$$

It is clear that as $q >> f^2$, the gain $\frac{z}{\eta} \to 1$, and as $q << f^2$, $\frac{z}{\eta} \to \frac{q}{f^2} \approx 0$. So one may say in general that low $\mathbf{Q}/\mathbf{R}$ ratio leads to the steady output gain that is smaller than one. To ensure the unity static gain, the demand needs to be scaled before entering the system. The lateral acceleration and roll rate demands, $\boldsymbol{\eta}(2)$, $\boldsymbol{\eta}(3)$ and $\boldsymbol{\eta}(4)$, need to be divided by $\mathbf{T}_{ss}(2,2)$ $\mathbf{T}_{ss}(3,3)$ and $\mathbf{T}_{ss}(4,4)$, respectively before entering the system.

In the following examples, we look at some of the selected runs with different dynamic pressure values, and examine their responses.

2.4 Step Responses at Different Operating Points

The simulations presented here are based on two flight scenarios – high and medium height launch modes. Given the altitude and Mach number, dynamic pressure $\bar{q}$ is computed as

$$\bar{q} = \frac{1}{2}\rho V^2 \tag{35}$$

where ρ and V are air density and speed. The dynamic pressure values are computed at various operating points along the flight envelopes, and are listed in Table 1 and Table 2.

Table 1: High Launch Flight Envelope

Altitude (m)	Mach No	Velocity (m/s)	Dynamic Pressure
30000	0.8	241	521
30000	2	604	3256
30000	4	1207	13026
30000	6	1811	29308
27500	8	2401	76102
25000	8.2	2448	117281
22500	8.4	2493	181313
20000	8.6	2538	283452
17500	8.8	2597	440208
15000	9	2656	682947
12500	9.2	2715	1058492
10000	9.4	2815	1637048
7500	9.6	2978	2470386
5000	9.8	3142	3635414
2500	10	3306	5232914
0	10.2	3451	7386198

Table 2: Medium Launch Flight Envelope

Altitude (m)	Mach No	Velocity (m/s)	Dynamic Pressure
15000	0.8	236	5396
20000	2	590	15330
25000	4	1194	27908
30000	6	1810	29308
30000	8	2415	52103
30000	10	3018	81411
27500	10	3002	118910
25000	10	2985	174422
22500	10	2968	256962
20000	10	2951	383250
17500	10	2951	568450
15000	10	2951	843144
12500	10	2951	1250581
10000	10	2995	1852703
7500	10	3102	2680540
5000	10	3206	3785313
2500	10	3306	5232914
0	10	3403	7099383

The open- and closed-loop responses at the selected operating points are simulated and the corresponding responses are examined. Firstly we present a quick look comparison between the open loop and closed loop responses, for a selected case where the altitude is 30 km and the Mach number is 2.

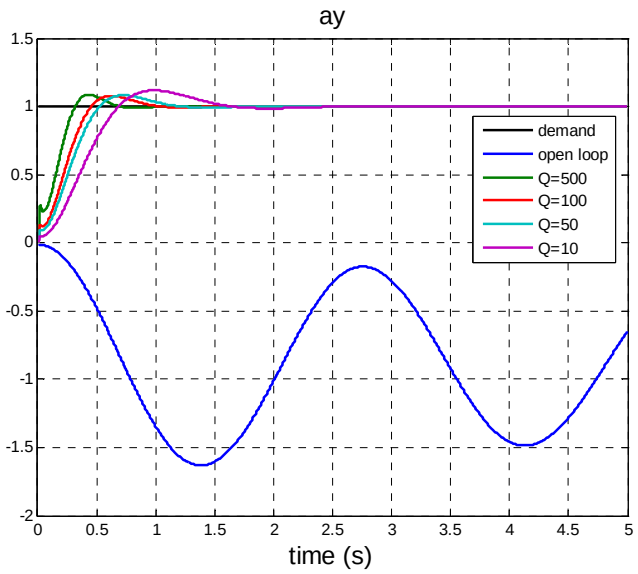

Figure 4: Open and closed loop responses. Open loop response is shown in blue

In Figure 4, the open loop response (blue) is a lightly damped oscillation, with a frequency of 2.29 rads^{-1}. This corresponds to the third dominant mode shown below. All of the poles have negative real parts, indicating that the system is open-loop stable.

Eigenvalue	**Damping**	**Freq. (rad/s)**
-3.65e-005	**1.00e+000**	**3.65e-005**
-6.26e-001	**1.00e+000**	**6.26e-001**
-7.90e-002 ± 2.29e+000i	**3.45e-002**	**2.29e+000**
:	**:**	**:**

Regarding the closed loop responses, all of them converge correctly to the demand. Note that the increase in **Q** results in a faster response. From (3), it is apparent that a higher **Q** setting puts more weight on reducing the sum of square of the gaps between $\boldsymbol{\eta}$ and $\mathbf{z}$ curves in Figure 5, hence resulting in a faster response.

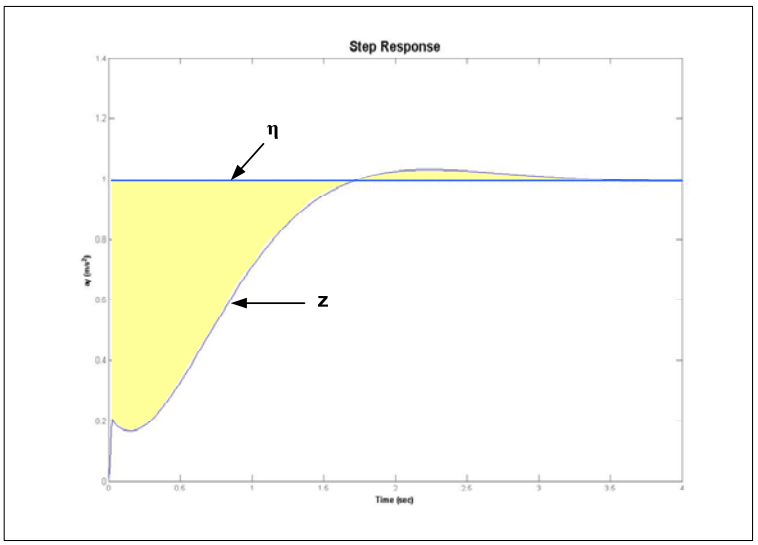

Figure 5: Larger Q means more weight on reducing the integral squares of the difference between $\boldsymbol{\eta}$ *and z curves. The shaded area shrinks as Q becomes larger.*

We now look at four examples of "high altitude low speed", "high altitude high speed", "medium altitude high speed", "low altitude high speed" cases.

Firstly for the high-altitude low-speed case, the step response is sluggish as shown in Figure 6, due to low dynamic pressure. It takes more than 3 seconds for the response to settle. Selecting high **Q** tends to speed up the convergence at the expense of slightly higher overshoot. The largest overshoot is about 8 percent. Note that it is important to make sure that the servo input values are feasible.

According to Bryson's rule [Franklin et. al. 2002], the first choice for the weighting matrices **Q** and **R** is to select diagonal **Q** and **R** with

$$\mathbf{Q}(i,i) = 1/(\text{maximum acceptible value of } \mathbf{e}(i)) \text{ where } i = \{1 \ldots 6\}, \text{ and}$$
$$\mathbf{R}(j,j) = 1/(\text{maximum acceptible value of } \mathbf{u}(j)) \text{ where } j = \{1,2,3\}.$$

Bryson's rule is often just the starting point to an iterative trial and error design procedure until the desired closed loop performance is achieved. In this report, we set $\mathbf{R} = \mathbf{I}$ and only vary $\mathbf{Q}$ as a scalar multiple of $\mathbf{I}$. The optimum **Q** is hand-picked as the one giving the fast response with small overshoot.

It is interesting to note that there is a sharp peak at the beginning of the rise. This is usually due to the existence of dominant closed-loop zeros in the left-half of the complex *s*-plane. We deal with these dominant zeros and their effects in the next section.

As for the high-altitude high-speed run (see Figure 7) the response is faster, reaching the steady state within 0.3 seconds. The overshoot is increased to about 10%. It is also noticed that the performance is consistent over a broad range of **Q** settings.

Another interesting observation is that the optimum **Q** value is smaller when the dynamic pressure is higher. The increase of the dynamic pressure causes the airframe to respond faster without having to increase the control effort.

Further increase in Mach number together with altitude reduction (see Figure 8) results in very large value of dynamic pressure. Again, this causes the optimum **Q** to become much smaller. The optimum **Q** is chosen as $0.0005\times\mathbf{I}$ (green) which results in the overshoot of 19% and the settling time of 0.08 second. Raising **Q** above $0.01\times\mathbf{I}$ introduces oscillations.

As for the low-altitude high-speed run (see Figure 9), the dynamic pressure is extremely high, leading to a very small **Q**. Again the green curve is picked as the optimum response ($\mathbf{Q}=1\times10^{-7}\mathbf{I}$). The settling time is less than 0.05 second, and the overshoot is about 15%.

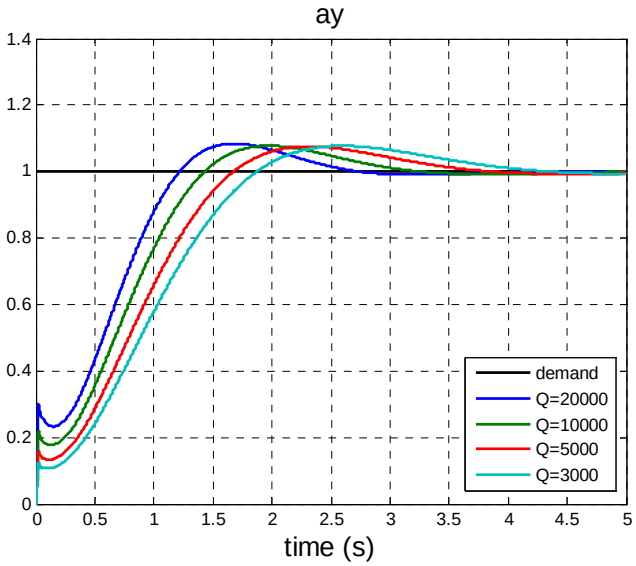

Figure 6: High altitude and low speed case (Start of Boost). 30 km, Mach 0.8, $\bar{q}=521$

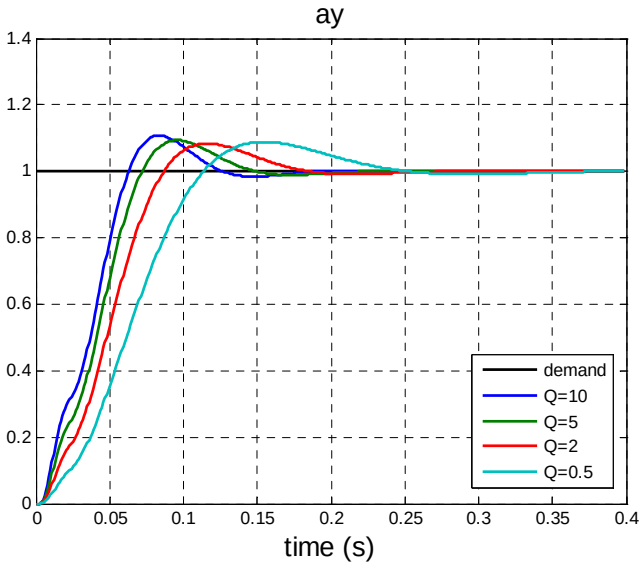

Figure 7: High altitude and high speed case (End of Boost). 30 km, Mach 6, $\bar{q}=29308$

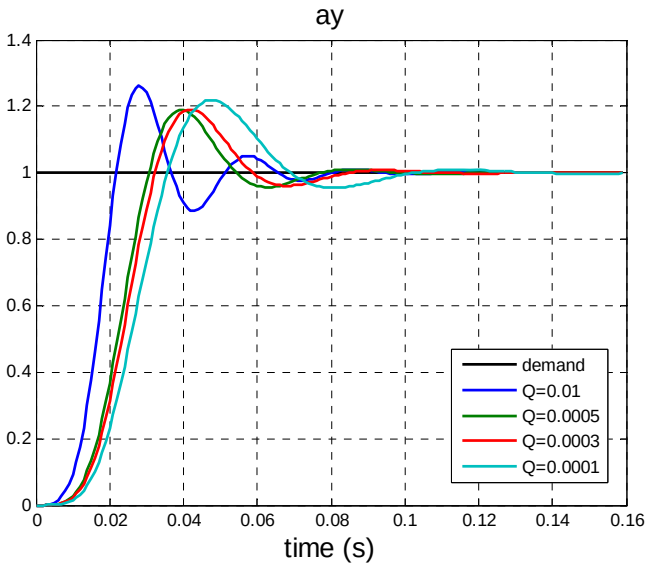

Figure 8: Medium altitude and high speed case (Dive). 15km, Mach 9, $\bar{q} = 682947$

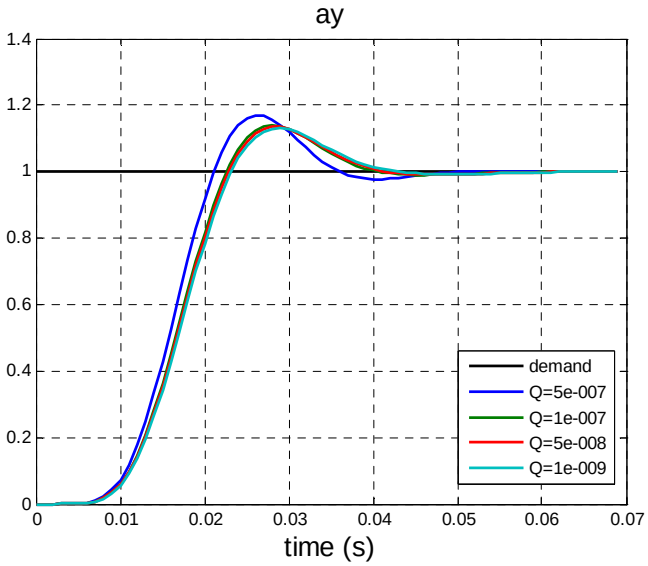

Figure 9: Low altitude and high speed case (Impact). 0km, Mach 10, $\bar{q} = 7386198$

2.5 Effect of Poles and Zeros on the Step Response

We select the high-altitude low-speed example in Section 2.4 to take a closer look at the initial positive bump in the step response. The transfer function a_y / a_{y_demand} is numerically given as

$$\frac{a_y}{a_{y\_demand}} = \frac{1.99\times10^{19}s^{17} + \cdots + 2.94\times10^{42}}{s^{21} + \cdots + 2.94\times10^{42}}$$

This transfer function has 21 poles and 17 zeros. After pole-zero cancellations, the transfer function is truncated to have only four most dominant poles $-2.66 \pm 2.24i$

and $-135.9 \pm 146.06i$, and two most dominant zeros $0.0004 \pm 4.66i$, before proceeding to the analysis of the effect of dominant zeros.

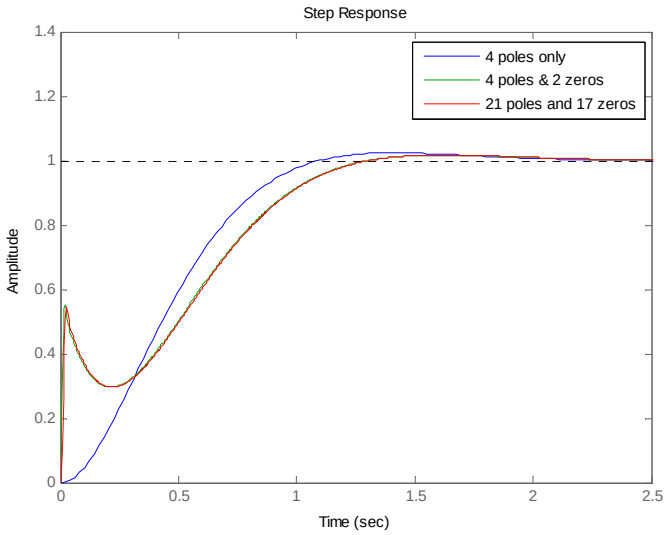

Figure 10: Step responses of truncated and original transfer functions: Blue-> [4 poles], Green-> [4 poles, 2 zeros], Red->[21 poles, 17 zeros].

Figure 10 indicates that the truncated model with 4 dominant poles and 2 dominant zeros is a good approximation – the green and red curves are well aligned. It is clear that the zeros are the most dominant. If we remove the zeros, the bump disappears (see the blue curve in Figure 10).

We want to examine how the movement of the zeros along the real and imaginary axes affects the initial bump. The simulation results are given in Figure 11 and Figure 12.

In Figure 11, as the zeros move away from the origin along the real axis, the initial bump becomes less prominent by means of the trough on the right being elevated, and eventually disappears (The cyan curve corresponds to the case when the zeros become less dominant than the poles). As the zeros move away from the origin along the imaginary axis, the actual height of the bumps drops and eventually disappears (see Figure 12).

Revisiting the higher speed run (Mach 6) as in Figure 7, the initial bump is significantly attenuated when compared with the slow speed run in Figure 6. For Figure 7, the dominant poles are $(-23.89 \pm 31.14i, -127.24 \pm 129.25i)$ and the dominant zeros are $(-0.24 \pm 95.7i)$. These zeros sit much further from the origin than the zeros in slow speed run of Figure 6, resulting in the diminished bump. This initial bump disappears as the dynamic pressure further increases.

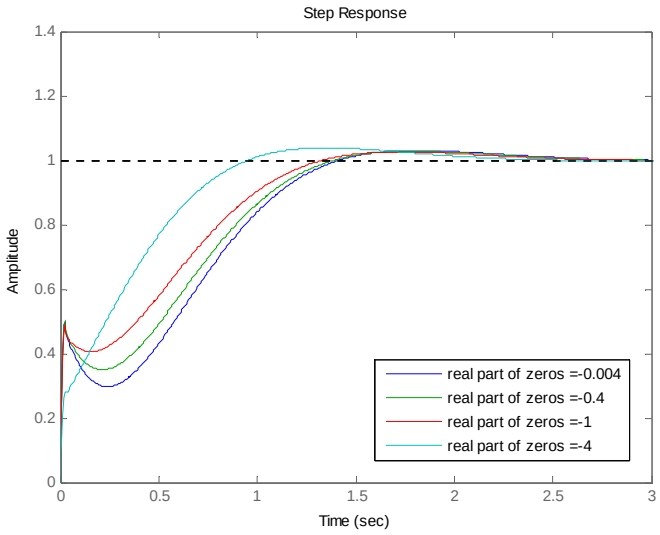

Figure 11: Effect of moving the zero along the real axis. The real part of zeros are: -0.004 (blue), -0.4 (green), -1 (red), and -4 (cyan).

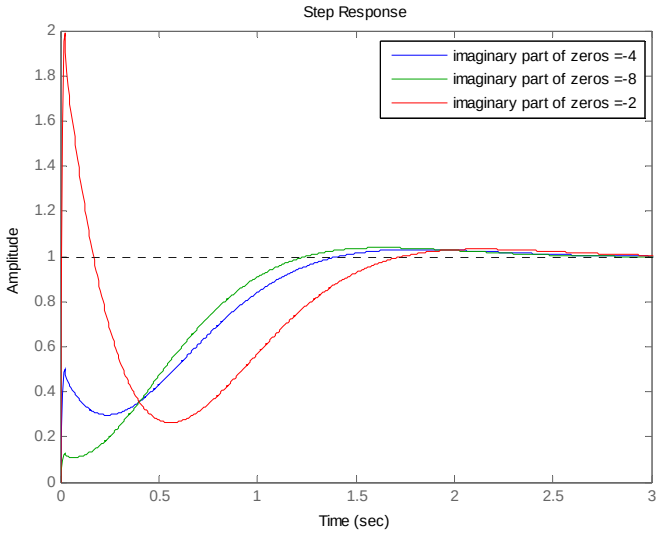

Figure 12: Effect of moving the zero along the imaginary axis. The imaginary part of zeros are: - ± 2 *(red),* ± 4 *(blue)and* ± 8 *(green).*

2.6 Why Positive Bump when Tail Controlled?

It is given in [Garnell and East 1977] that the IMU is mounted 0.5 m fore of the missile centre of gravity (CG). We define d_x as the IMU displacement from the CG along the missile's forward axis (e.g., d_x=0.5). Considering the most sluggish response in the high-altitude low-speed case, the y-axis linear acceleration and z-axis (yaw) angular acceleration are plotted in Figure 13. The initial transient portions (red-circle) are zoomed for a closer look. A negative rudder deflection as in Figure 14 (ie., anticlockwise when viewed from above) initially pushes the missile to the left before the clockwise rotation steers it to right. Therefore the sensor at the CG should experience a brief negative y-acceleration first and then a positive y-

acceleration. This phenomenon is known as non-minimum phase response which often arises among the tail-controlled missiles.

The positive bump in Figure 13 is the result of the accelerometer being placed fore of the CG, hence sensing the lever arm effect. The positive angular acceleration (right plot in Figure 13) translates to the positive linear acceleration (e.g., $a_y = d_x \dot{r}$) that happens to be greater than the initial negative bump.

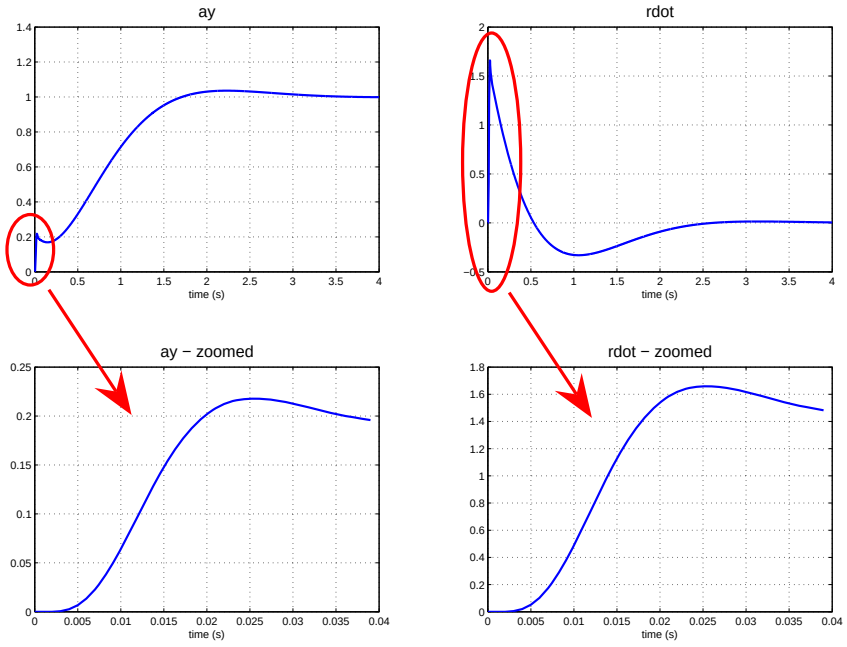

Figure 13: a_y (y acceleration) and $\dot{r}$ (yaw acceleration) responses. The plots on the bottom are the enlarged initial responses.

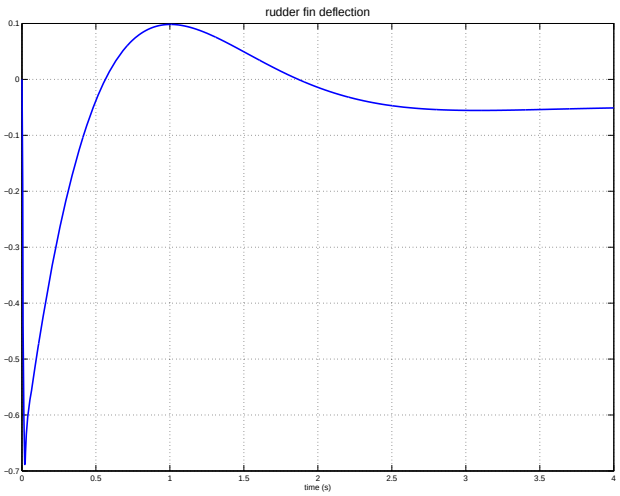

Figure 14: Rudder fin deflection

As mentioned earlier, the rudder fin deflection is mostly negative in Figure 14. The fact that the negative fin deflection leads to the positive yaw motion confirms that the missile is tail-controlled. Another way to prove that the missile is tail-controlled, is to shift the IMU back to the CG (i.e., d_x=0) and show that the initial bump becomes negative. In Figure 15, without the lever arm effect, the initial y-acceleration bump is negative (peaked to about -0.5 m/s²) as expected. Adding this -0.5 m/s² to lever-arm effect ($\approx$0.8 m/s²) gives a net acceleration of 0.3 m/s². This value is similar to the 0.2 m/s² bump in Figure 13. Furthermore, it is also shown that shifting the IMU to the CG results in one of the zeros becoming positive as shown Figure 16.

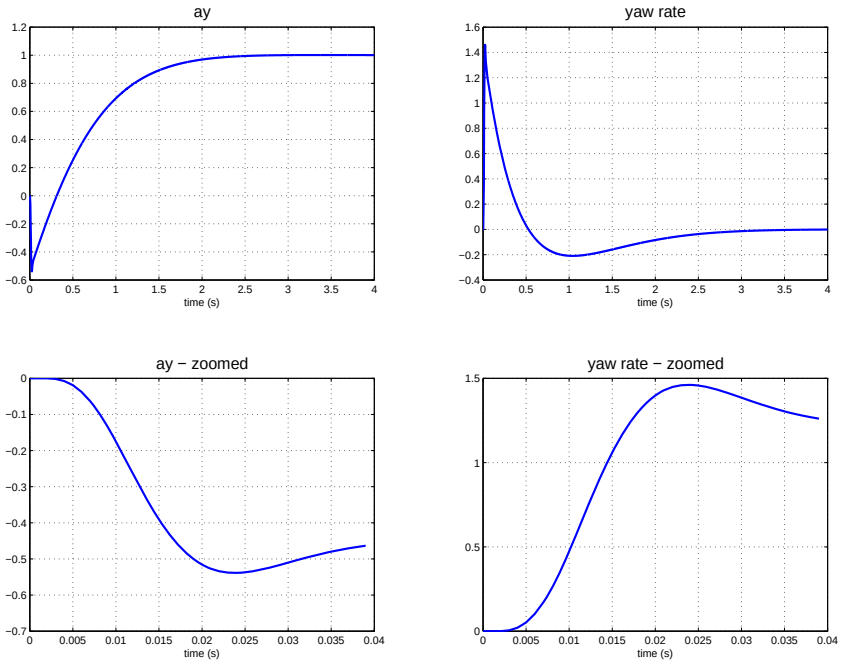

Figure 15: Non-minimum phase response for y-acceleration and the associated angular acceleration, when the IMU is at the CG. Bottom row is the zooming of the initial bumps in the top row.

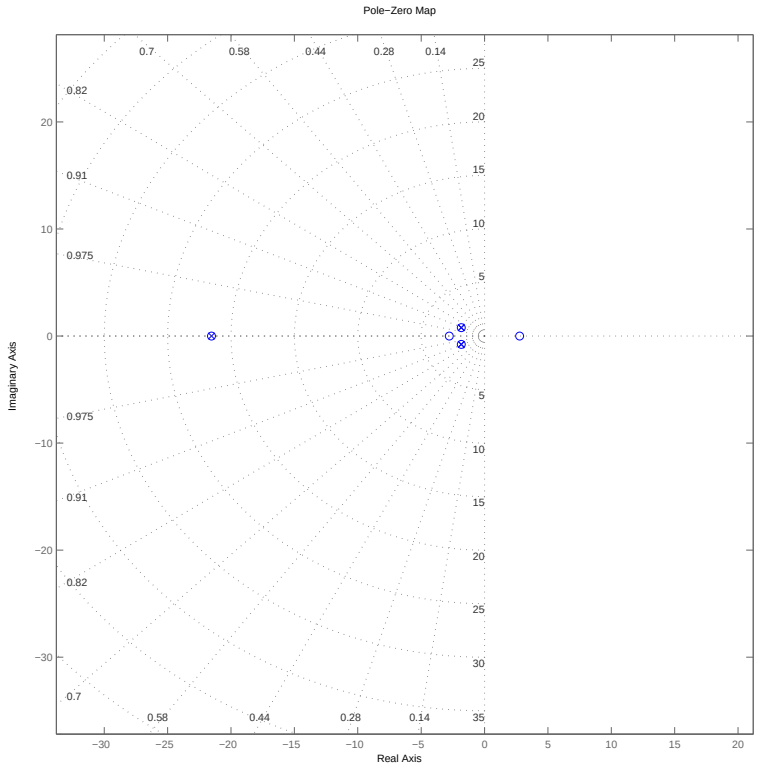

Figure 16: Pole and zero plot when the IMU is at the CG. Poles are shown as crosses and zeros are shown as circles.

2.7 Gain Scheduling – Optimal Weight versus Dynamic Pressure

Gain scheduling is an approach that uses a family of linear controllers, each of which provides satisfactory control at its operating point. The scheduling variables are defined as parameters used to determine the operating point the system is currently at. In a flight control system, they are usually the altitude and Mach number as given in Tables 1-2. This is one of the simplest and most intuitive forms of adaptive control (strictly speaking this is not adaptive as the system does not have self-organising features).

For a given dynamic pressure, we iterate the step response simulations over various **Q** settings and hand-pick the optimum **Q**. The optimal **Q** values are then plotted against their dynamic pressure counterparts The log-log plot in Figure 17 exhibits a one-to-one mapping, suggesting that the dynamic pressure may be used as the single gain-scheduling input for the flight envelope of consideration.

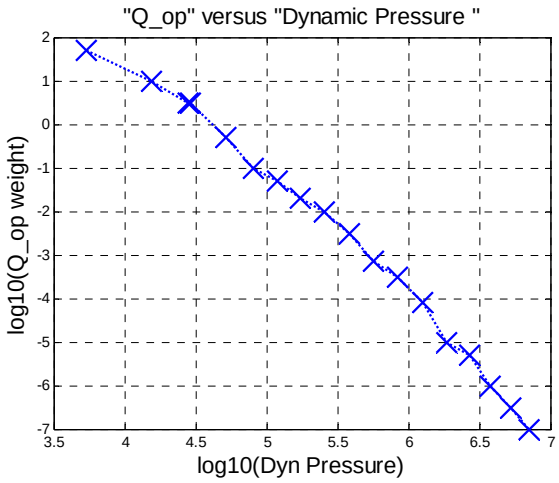

Figure 17: Optimum Q versus dynamic pressure

3. Output Feedback Control System

3.1 Formulation

In the earlier stages of control design, we assumed that all the states were accurately measureable. This assumption does not hold in practice. In the given model, 6 out of the 24 states are actually measurable (ie., IMU outputs). Therefore, it is appropriate to include a state observer design as shown in Figure 18.

The state observer estimates all 24 states including the six measurable ones (ie., full state observer) by adjusting the filter gain $\mathbf{K}_f$ so that the measurement difference $(\mathbf{z} - \mathbf{J}\hat{\mathbf{x}})$ remains small.

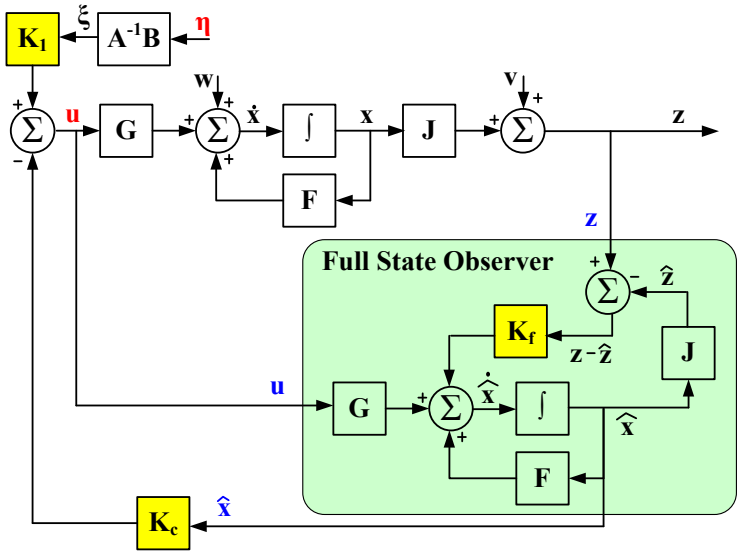

Figure 18: Observed-state feedback control system

In order to derive the state observer, we first consider the plant and measurement equations

$$\dot{\mathbf{x}} = \mathbf{F}\mathbf{x} + \mathbf{G}\mathbf{u} \tag{36}$$

$$\mathbf{z} = \mathbf{J}\mathbf{x}. \tag{37}$$

Suppose we construct the dynamic equations for the estimated state $\hat{\mathbf{x}}$ by replicating (36).

$$\dot{\hat{\mathbf{x}}} = \mathbf{F}\hat{\mathbf{x}} + \mathbf{G}\mathbf{u} \tag{38}$$

Now define the estimation error as $\mathbf{e}_x = \mathbf{x} - \hat{\mathbf{x}}$, and derive the error propagation equation. Subtracting (38) from (36), we arrive at

$$\dot{\mathbf{e}}_x = \dot{\mathbf{x}} - \dot{\hat{\mathbf{x}}} = \mathbf{F}\mathbf{x} - \mathbf{F}\hat{\mathbf{x}} = \mathbf{F}\mathbf{e}_x. \tag{39}$$

This shows that when the matrix $\mathbf{F}$ is asymptotically stable, the error $\mathbf{e}_x$ converges to zero for any input $\mathbf{u}$, which means that $\hat{\mathbf{x}}$ eventually converges to $\mathbf{x}$ as $t \to \infty$. However, when $\mathbf{F}$ is not stable, $\mathbf{e}_x$ is unbounded and $\hat{\mathbf{x}}$ may grow very large. To avoid this, one must add a correctional term to (38) as shown below.

$$\dot{\hat{\mathbf{x}}} = \mathbf{F}\hat{\mathbf{x}} + \mathbf{G}\mathbf{u} + \mathbf{K}_f(\mathbf{z} - \mathbf{J}\hat{\mathbf{x}}) \tag{40}$$

where $\mathbf{K}_f$ is a 24×6 filter gain matrix.

When $\hat{\mathbf{x}}$ becomes very close to $\mathbf{x}$, the correctional term $\mathbf{K}_f(\mathbf{z} - \mathbf{J}\hat{\mathbf{x}})$ plays minimum role. However, when $\hat{\mathbf{x}}$ drifts away from $\mathbf{x}$, the role of this term (driving $\hat{\mathbf{x}}$ towards $\mathbf{x}$) becomes more dominant.

To see how this can be done, the error propagation equation is given by subtracting (40) from (36),

$$\dot{\mathbf{e}}_x = \dot{\mathbf{x}} - \dot{\hat{\mathbf{x}}} = (\mathbf{F} - \mathbf{K}_f\mathbf{J})\mathbf{e}_x \tag{41}$$

Now $\mathbf{e}_x$ converges to zero as long as $(\mathbf{F} - \mathbf{K}_f\mathbf{J})$ is asymptotically stable. We know that even if $\mathbf{F}$ is unstable, we can find $\mathbf{K}_f$ that makes $(\mathbf{F} - \mathbf{K}_f\mathbf{J})$ stable. The system (40) can also be expressed as

$$\dot{\hat{\mathbf{x}}} = (\mathbf{F} - \mathbf{K}_f\mathbf{J})\hat{\mathbf{x}} + \mathbf{G}\mathbf{u} + \mathbf{K}_f\mathbf{z} \tag{42}$$

This state observer has two inputs – the plant input $\mathbf{u}$ and the measurement output $\mathbf{z}$ as shown in Figure 18.

Any choice of $\mathbf{K}_f$ in (42) for which $(\mathbf{F} - \mathbf{K}_f\mathbf{J})$ is asymptotically stable will make $\hat{\mathbf{x}}$ converge to $\mathbf{x}$. However, in general the output $\mathbf{z}$ and the process dynamics are contaminated by measurement noise and disturbance (process noise) respectively, therefore a more realistic model representation would be

$$\dot{\mathbf{x}} = \mathbf{F}\mathbf{x} + \mathbf{G}\mathbf{u} + \mathbf{w} \tag{43}$$
$$\mathbf{z} = \mathbf{J}\mathbf{x} + \mathbf{v} \tag{44}$$

The process and measurement noises **w** and **v** are assumed Gaussian and satisfy

$$E(\mathbf{w}) = \mathbf{0}, E(\mathbf{v}) = \mathbf{0}, E(\mathbf{w}\mathbf{w}^T) = \mathbf{Q}_\mathrm{f}, \text{ and } E(\mathbf{v}\mathbf{v}^T) = \mathbf{R}_\mathrm{f}, \tag{45}$$

Including the error terms, the error dynamics in (41) can be rewritten as

$$\begin{aligned}\dot{\mathbf{e}}_\mathrm{x} &= \mathbf{F}\mathbf{x} + \mathbf{w} - (\mathbf{F} - \mathbf{K}_\mathrm{f}\mathbf{J})\hat{\mathbf{x}} - \mathbf{K}_\mathrm{f}(\mathbf{J}\mathbf{x} + \mathbf{v}) \\ &= (\mathbf{F} - \mathbf{K}_\mathrm{f}\mathbf{J})\mathbf{e}_\mathrm{x} + \mathbf{w} - \mathbf{K}_\mathrm{f}\mathbf{v}.\end{aligned} \tag{46}$$

Because of **w** and **v**, the estimation errors may not converge to zero, but may become very small if the right $\mathbf{K}_\mathrm{f}$ is selected. This motivates the so-called Linear Quadratic Gaussian (LQG) estimation problem.

The objective is to find $\mathbf{K}_\mathrm{f}$ that drives the following error covariance to the minimum.

$$\mathbf{P}_\mathrm{f} = E(\mathbf{e}_\mathrm{x}\mathbf{e}_\mathrm{x}^T), \tag{47}$$

Note that $\mathbf{P}_\mathrm{f}$ is symmetric and positive semi-definite. Solving the LQG problem leads to the differential Riccati equation given as

$$\dot{\mathbf{P}}_\mathrm{f} = \mathbf{F}\mathbf{P}_\mathrm{f} + \mathbf{P}_\mathrm{f}\mathbf{F}^T - \mathbf{P}_\mathrm{f}\mathbf{J}^T\mathbf{R}_\mathrm{f}^{-1}\mathbf{J}\mathbf{P}_\mathrm{f} + \mathbf{Q}_\mathrm{f} \tag{48}$$

which is solved forward in time with the initial condition of $\mathbf{P}_\mathrm{f}(t_0)$.

If the observer is stable, then we may set $t_0 = -\infty$, and obtain the steady state solution by solving the filtering algebraic Ricatti equation (FARE)

$$\mathbf{0} = \mathbf{F}\mathbf{P}_\mathrm{f} + \mathbf{P}_\mathrm{f}\mathbf{F}^T - \mathbf{P}_\mathrm{f}\mathbf{J}^T\mathbf{R}_\mathrm{f}^{-1}\mathbf{J}\mathbf{P}_\mathrm{f} + \mathbf{Q}_\mathrm{f} \tag{49}$$

Using the analogy of this equation (FARE) with the previous CARE in the LQR design, the analytic method of [Naidu 2002] or matlab function *care* can be used again to generate $\mathbf{P}_\mathrm{f}$.

$$\mathbf{P}_\mathrm{f} = care(\mathbf{F}^T, \mathbf{J}^T, \mathbf{Q}_\mathrm{f}, \mathbf{R}_\mathrm{f})$$

And the optimal filter gain $\mathbf{K}_\mathrm{f}$ is given as

$$\mathbf{K}_\mathrm{f} = \mathbf{P}_\mathrm{f}\mathbf{J}^T\mathbf{R}_\mathrm{f}^{-1}. \tag{50}$$

3.2 Simulation

Having found the optimal $\mathbf{K}_\mathrm{f}$, the state observer takes the measurements and the control input, and estimates the states. In this section, we repeat the first two examples in Section 2.4 to observe the effect of including the state observer on the performance. The simulation results are shown in Figure 19 and Figure 20.

The errors $\mathbf{w}$ and $\mathbf{v}$ are given as Gaussian noises $[\mu = 0, \sigma = 0.01]$ and their covariance matrices are set as

$$\mathbf{Q}_\mathrm{f} = 10^{-3}\,\mathbf{I}_{24\times 24}$$
$$\mathbf{R}_\mathrm{f} = 10^{-4}\,\mathbf{I}_{6\times 6}$$

Figure 19 and Figure 20 indicate that all the excited states are estimated well. For benign states (ie., appearing as noises), their estimates are simply the noise-attenuated. In all cases, no estimate breaks away from the true states, suggesting that $\mathbf{F} - \mathbf{K}_\mathrm{f}\mathbf{J}$ in (46) is stable. It was also observed that a very high $\mathbf{Q}_\mathrm{f} / \mathbf{R}_\mathrm{f}$ ratio often leads to instability.

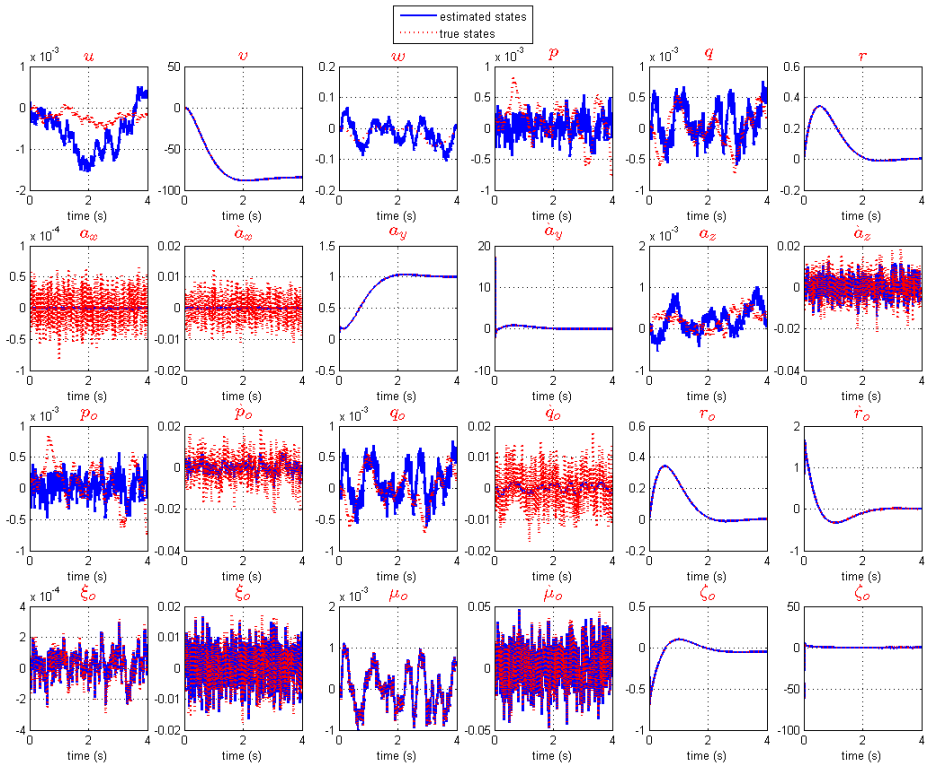

Figure 19: Plot of the 24 estimated states (blue) versus the true states(red) for the high altitude low speed run with Q=10000

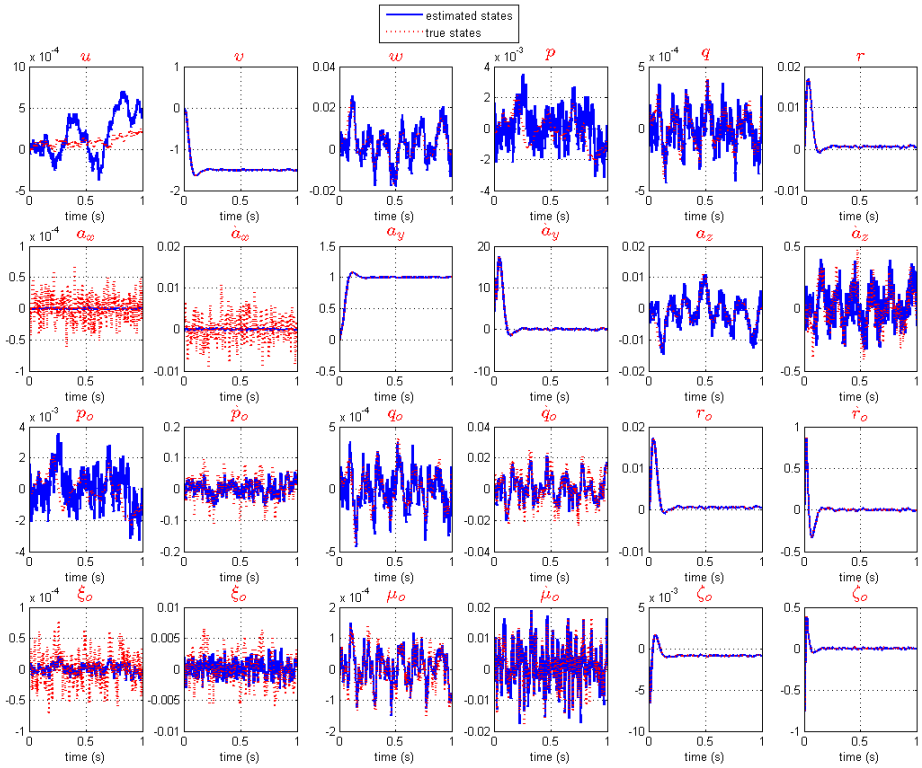

Figure 20: Plot of the 24 estimated states (blue) and the true states(red) for the high altitude and high speed run with Q=2.

3.3 Effect of Adding the Observer on Closed Loop System

The step responses of the output feedback system are similar to those of the state feedback system. It appears that the dynamical behaviours of the closed loop system are not largely affected by inclusion of the state observer.

Since the dynamical behaviour is solely due to the pole locations, we can ignore the input gain terms for the following analysis. We revisit the process equation (36) with the feedback input $\mathbf{u} = -\mathbf{K}_c\hat{\mathbf{x}}$ and also the estimation error differential equation (41).

$$\begin{aligned}\dot{\mathbf{x}} &= \mathbf{F}\mathbf{x} + \mathbf{G}(-\mathbf{K}_c\hat{\mathbf{x}}) \\ &= \mathbf{F}\mathbf{x} - \mathbf{G}\mathbf{K}_c(\mathbf{x} - \mathbf{e}_x) \\ &= (\mathbf{F} - \mathbf{G}\mathbf{K}_c)\mathbf{x} + \mathbf{G}\mathbf{K}_c\mathbf{e}_x\end{aligned} \tag{51}$$

$$\begin{aligned}\dot{\mathbf{e}}_x &= \mathbf{F}\mathbf{x} - \mathbf{F}\hat{\mathbf{x}} \\ &= (\mathbf{F} - \mathbf{K}_f\mathbf{J})\mathbf{e}_x\end{aligned} \tag{52}$$

The above equations can be combined in single matrix notation as

$$\begin{bmatrix} \dot{\mathbf{x}} \\ \dot{\mathbf{e}}_x \end{bmatrix} = \begin{bmatrix} \mathbf{F} - \mathbf{G}\mathbf{K}_c & \mathbf{G}\mathbf{K}_c \\ \mathbf{0} & \mathbf{F} - \mathbf{K}_f\mathbf{J} \end{bmatrix} \begin{bmatrix} \mathbf{x} \\ \mathbf{e}_x \end{bmatrix}. \tag{53}$$

The above equation describes the dynamical behaviour of the output feedback control system. The characteristic equation becomes

$$\begin{vmatrix} s\mathbf{I} - (\mathbf{F} - \mathbf{G}\mathbf{K}_c) & -\mathbf{G}\mathbf{K}_c \\ \mathbf{0} & s\mathbf{I} - (\mathbf{F} - \mathbf{K}_f\mathbf{J}) \end{vmatrix} = \left| s\mathbf{I} - (\mathbf{F} - \mathbf{G}\mathbf{K}_c) \right| \left| s\mathbf{I} - (\mathbf{F} - \mathbf{K}_f\mathbf{J}) \right| = 0 . \tag{54}$$

The closed-loop poles of the combined system are a *union* of the two independent groups of poles – one belonging to the regulator dynamics $\mathbf{F} - \mathbf{G}\mathbf{K}_c$ and the other belonging to the state observer dynamics $\mathbf{F} - \mathbf{K}_f\mathbf{J}$. The observer does not shift the pole locations of the regulator, hence making it possible to design the regulator and observer separately and bring them together later. This property is known as the *Separation Principle* [Anderson and Moore 1989]. If both the matrices are asymptotically stable, then so will be the closed-loop system.

From the steady state point of view, inclusion of the estimator makes no difference (because $\mathbf{e} \to \mathbf{0}$). From the transient point of view, the behaviour of the combined system might be different from that of the true-state feedback system. Ideally, the poles of $\mathbf{F} - \mathbf{K}_f\mathbf{J}$ should be placed to the left of the poles of $\mathbf{F} - \mathbf{G}\mathbf{K}_c$ so that the observer response is faster than the regulator response.

The current setting of $\mathbf{R}_f$ and $\mathbf{Q}_f$ results in the observer poles placed to the left of the regulator poles (dominant poles are shown below), and there is no apparent detrimental effects from the observer poles on the overall system dynamics. Further experiments indicated that in order to separate the observer poles further from the regulator poles, the $\mathbf{Q}_f / \mathbf{R}_f$ ratio needs to increase further, which speeds up the estimation convergence. As stated before, increasing $\mathbf{Q}_f / \mathbf{R}_f$ excessively leads to instability.

Low Speed

Observer poles	Regulator poles
-0.00018202	-5.8343e-006
-2.6 ± 1.6e-014i	-1.5082 ± 1.5075i

High Speed

Observer poles	Regulator poles
-0.0010883	-0.00032818
-43.708	-18.03
-41.544 ± 57.937i	-23.887 ± 31.142i

4. Conclusions

We present an optimal flight control design where the objective is to find a feedback gain that achieves a good balance of fast response and small control effort. We adopt the generic 24-state airframe model derived in [Farhan 2007], and the aerodynamic coefficients are taken from the open literature [Garnell and East 1977] where the missile is symmetric and has a cruciform shape.

Initially, effects of varying the weighting matrix $\mathbf{Q}$ on the step responses were investigated. It was concluded that increasing $\mathbf{Q}$ improves the response speed but at the expense of increased control burden. The closed loop responses were examined at numerous operating points along the flight envelope, and the corresponding optimum $\mathbf{Q}$ values are noted. When the dynamic pressure becomes high, reducing the control effort becomes the primary objective as the fast response is readily achievable. It looks feasible to use the dynamic pressure as a sole gain-scheduling input for the flight envelope of consideration.

The dominant zeros affect the initial transient of the step response. Tail-controlled missiles are expected to exhibit non-minimum phase responses. However, having the IMU placed sufficiently ahead of the CG, allows the positive zero(s) of the transfer function $(a_{\text{y\_out}} / a_{\text{y\_desired}})$ to become negative, reversing the sign of the initial bump.

The design and simulation of an LQG controller are also presented. When the process noise covariance $\mathbf{Q}_{\text{f}}$ is made larger than the measurement noise covariance $\mathbf{R}_{\text{f}}$, the estimator interprets a large deviation of $\hat{\mathbf{z}}$ from $\mathbf{z}$ as an indication that the estimate $\hat{\mathbf{x}}$ is poor hence needs to be aggressively corrected. In practice, this leads to large $\mathbf{K}_{\text{f}}$ and fast poles for $\mathbf{F} - \mathbf{K}_{\text{f}}\mathbf{J}$ leading to fast convergence. Making $\mathbf{Q}_{\text{f}}$ excessively large, however, makes the system unstable. Overall, the inclusion of the state observer does not seem to deteriorate the tracking performance.

The LQR based controller is relatively easy to implement on multivariable systems, and the closed loop system is asymptotically stable. The tuning process is a simple adjustment of $\mathbf{Q}/\mathbf{R}$ ratio until the desired balance of fast response and small control effort is achieved.

5. References

1. Anderson, B. R. O. and Moore, J. B., "*Optimal Control – Linear Quadratic Methods*", Prentice-Hall International, Inc, 1989.

2. Faruqi, F. A., "*State Space Model for Autopilot Design of Aerospace Vehicles*", DSTO-TR-1990, March, 2007.

3. Franklin, G. F, Powell, J. D., and Emami-Naeini, A., "*Feedback Control of Dynamic Systems*", Prentice Hall, Upper Saddle River, NJ, 4th edition, 2002.

4. Garnell, P. and East, D. J., "*Guided Weapon Control Systems*", Pergamon Press, 1977.

5. Naidu, D. S., "*Optimal Control Systems*", CRC Press, 2002.

6. Nesline, F. W. and Nabbefeld, N. C, "*Design of digital autopilots for homing missile*", Proceedings of American Control Conference, San Diego, California, USA, June 6-8, pp 716-730, 1984.

7. Ogata, K., "*Modern Control Engineering (2nd Edition)*", Prentice Hall, 1995.

8. Sage, A. P., "*Optimum Systems Control*", Prentice Hall, INC, 1968.

9. Simon, D., "*Optimal State Estimation: Kalman, H infinity, and Nonlinear Approaches*", John Wiley & Sons, Inc., 2006.

DEFENCE SCIENCE AND TECHNOLOGY ORGANISATION
DOCUMENT CONTROL DATA

1. PRIVACY MARKING / CAVEAT (OF DOCUMENT)

2. TITLE

Design of Optimal Flight Controller for Generic Linearised Missile Model in Hypersonic Regime

3. SECURITY CLASSIFICATION (FOR UNCLASSIFIED REPORTS THAT ARE LIMITED RELEASE USE (L) NEXT TO DOCUMENT CLASSIFICATION)

Document	(U)
Title	(U)
Abstract	(U)

4. AUTHOR(S)

Jijoong Kim and Farhan A. Faruqi

5. CORPORATE AUTHOR

DSTO Defence Science and Technology Organisation
PO Box 1500
Edinburgh South Australia 5111 Australia

6a. DSTO NUMBER	6b. AR NUMBER	6c. TYPE OF REPORT	7. DOCUMENT DATE
DSTO-TR-2423	AR-017-787	Technical Report	July 2010

8. FILE NUMBER	9. TASK NUMBER	10. TASK SPONSOR	11. NO. OF PAGES	12. NO. OF REFERENCES
2009 / 1101832	07 / 249	CWSD	26	9

13. URL on the World Wide Web

http://www.dsto.defence.gov.au/corporate/reports/DSTO-TR-2423.pdf

14. RELEASE AUTHORITY

Chief, Weapons Systems Division

15. SECONDARY RELEASE STATEMENT OF THIS DOCUMENT

Approved for public release

OVERSEAS ENQUIRIES OUTSIDE STATED LIMITATIONS SHOULD BE REFERRED THROUGH DOCUMENT EXCHANGE, PO BOX 1500, EDINBURGH, SA 5111

16. DELIBERATE ANNOUNCEMENT

No Limitations

17. CITATION IN OTHER DOCUMENTS Yes

18. DSTO RESEARCH LIBRARY THESAURUS http://web-vic.dsto.defence.gov.au/workareas/library/resources/dsto_thesaurus.shtml

flight control, linear system, optimal control, state observer

19. ABSTRACT

This report presents a multivariable controller design for a generic missile travelling at hypersonic speed. The controller is based on the theory of optimal control, and the solution is provided by a feedback controller known as a Linear Quadratic Regulator (LQR) for tracking the demands (lateral acceleration and roll rate) as closely as possible while keeping the actuator efforts (for deflecting aileron, elevator and rudder) small. In the computer simulation, the missile model is subject to various hypersonic flight conditions and gain scheduling is exercised as a function of dynamic pressure. The intial study assumes perfect knowledge of all the states for the controller design. Subsequently, a state observer (kalman filter) is introduced into the design to reflect a more practical synthesis where some of the states need to be estimated.